Design of filtering microstrip antenna array with reduced sidelobe level

Chen, Fu-chang; Hu, Hao-tao; Li, Run-shuo; Chu, Qing-xin; Lancaster, Michael J.

DOI:
10.1109/TAP.2016.2639469

Document Version
Peer reviewed version

Citation for published version (Harvard):
Chen, F, Hu, H, Li, R, Chu, Q & Lancaster, MJ 2017, 'Design of filtering microstrip antenna array with reduced sidelobe level', *IEEE Transactions on Antennas and Propagation*, vol. 65, no. 2, pp. 903-908. https://doi.org/10.1109/TAP.2016.2639469

Design of Filtering Microstrip Antenna Array with Reduced Sidelobe Level

Fu-Chang Chen, Hao-Tao Hu, Run-Shuo Li, Qing-Xin Chu, and Michael J. Lancaster

***Abstract*—For the requirements of efficient integration and simple fabrication, a new co-design approach for a microstrip filter with an antenna array with reduced sidelobe level is introduced in this paper. The microstrip patch antennas and the stub-loaded resonators are used to illustrate the synthesis of a bandpass filtering antenna array. By controlling the coupling strength between the resonators, a uniform or non-uniform power divider network can be obtained. A non-uniform power division is used to reduce the sidelobe level. The equivalent lumped circuit model is developed and analyzed in detail. Two types of eight-element filtering antenna array with uniform and tapered power-distribution among the elements have been designed. Simulated and measured results provide a good verification for the theoretical concepts.**

***Index Terms*—Filtering antenna array, low sidelobe, microstrip antenna, patch antenna, stub-loaded resonator.**

I. Introduction

With the rapid development of wireless communication technology multifunctional component design has become increasingly of interest. As the key components in most of the RF front ends, the bandpass filter and the antenna are usually designed separately and connected by a 50-Ω transmission line, which not only increases the volume but also maybe degrades in-band performance due to the mismatch and extra insertion loss caused by the interconnections.

Recently, a co-design approach has been proposed to integrate the bandpass filter and the antenna into a single component, so called *filtering antenna*, with filtering and radiating functions simultaneously. So far several filtering antennas in different forms, such as Γ-shaped monopole antennas [1] [2], rectangular patch antennas [3] [4], fan-shaped patch antenna [5] and substrate integrated waveguide (SIW) slot antenna [6] have been designed. Using step impedance resonators, a compact dual-band filtering patch antenna is reported in [7]. In [8], a compact high-gain filtering patch antenna without extra filtering circuits is investigated.

The study of filtering antenna with single radiating element is well developed. As for the filtering antenna array, some design methods have also been proposed. The simplest one is cascading the antenna array with a band-pass filter, but often at the cost of increasing the volume and degrading the in-band performance as mentioned previously. To avoid this problem, another possible method is to replace the radiating elements by the filtering antennas [9]. If the radiating elements in the array have the filtering function, then only the signals in desired bands could be received/transmitted by the antenna array. In [10], a filtering microstrip antenna array is realized by designing the feeding network with both the functions of power division and band selection. Although the filtering antenna arrays in [9] and [10] exhibit good filtering response, the sidelobe level is not satisfactory. This is due to the uniform power division of the feeding network. It is worth mentioning that not only the filtering property but also the low sidelobe level is important for the antenna array to select the desired signals (at desired frequency, in desired direction).

In this paper, a design of an eight-element filtering microstrip antenna array with reduced sidelobe level is presented. The operating principles, synthesis equations, and design graphs are first introduced. Two filtering antenna arrays are investigated, one is fed by a uniform power distribution the other a non-uniform power distribution. This is the first time a filtering antenna array with tapered power-distribution has been presented. Compared with the uniform filtering antenna array, the one with tapered power-distribution features a lower sidelobe performance. Both the antenna arrays show sharp band-edge characteristic, flat antenna gain in the passband and high suppression in the stopband.

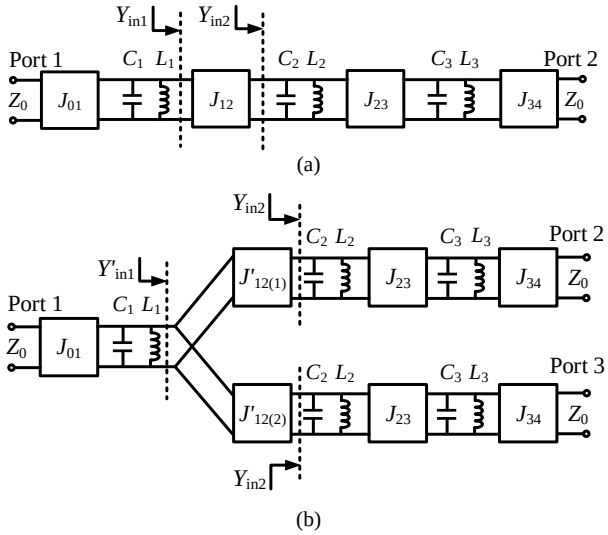

Fig. 1. Typical third-order band-pass filter (a) and third-order filtering uniform/non-uniform power divider (b).

II. Structure and Equivalent Model

Fig. 1 depicts a typical network of a third-order bandpass filter and a filtering power divider. All the resonators and admittance inverters in power divider network are correspondingly equal to those in filter network except the

This work was supported by the National Natural Science Foundation of China under Grant 61327005 and Grant 61571194, by the Project of the Pearl River Young Talents of Science and Technology in Guangzhou under Grant 201610010095, by the Foundation for Distinguished Young Talents in Higher Education of Guangdong, by the Science and Technology Planning Project of Guangdong Province under Grant 2014A010103013, by the Natural Science Foundation of Guangdong Province under Grant 2015A030313203, and by the Fundamental Research Funds for the Central Universities under Grant 2015ZZ093 and Grant 2015ZM066.

F. C. Chen, H. T. Hu, R. S. Li, and Q. X. Chu are with the School of Electronic and Information Engineering, South China University of Technology, Guangzhou 510641, China (e-mail: chenfuchang@scut.edu.cn).

M. J. Lancaster is with the School of Electronics, Electrical and Systems Engineering, University of Birmingham, Birmingham B15 2TT, U.K.

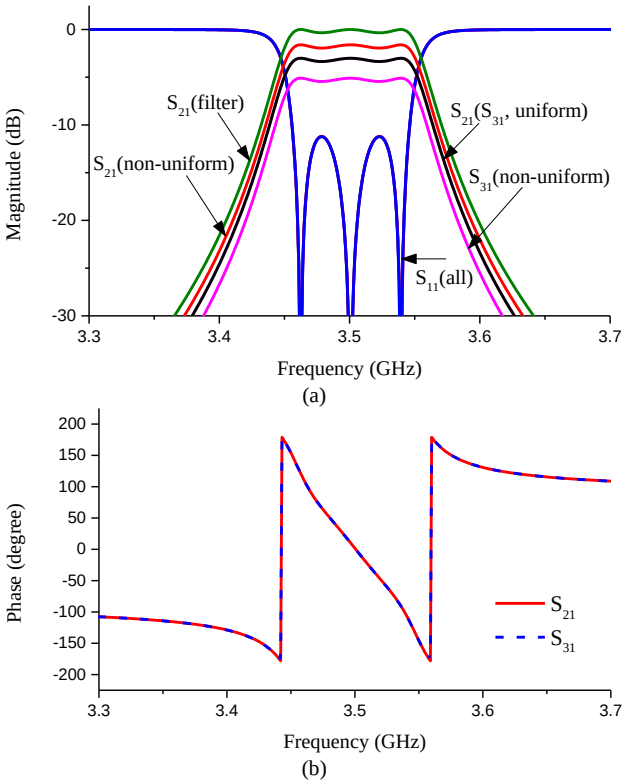

Fig. 2. (a) S-parameters of different situations of the power divider compared to those of the typical third-order band-pass filter. (b) The phase response of the two transmission paths of the non-uniform power divider.

admittance inverters $J'_{12(1)}$ and $J'_{12(2)}$. The input admittance Y_{in1} is calculated as [11]

$$Y_{in1} = J_{12}^2 / Y_{in2} \tag{1}$$

Similarly, the input admittance Y'_{in1} is obtained as

$$Y'_{in1} = J'^2_{12(1)} / Y_{in2} + J'^2_{12(2)} / Y_{in2} \tag{2}$$

To make the power divider and the filter exhibit the same reflection coefficient, the above two input admittance Y_{in1} and Y'_{in1} should keep the same. Thus, making equation (1) equal to (2) gives

$$J_{12}^2 = J'^2_{12(1)} + J'^2_{12(2)} \tag{3}$$

When admittance inverters $J'_{12(1)}$ and $J'_{12(2)}$ are identical, the divider is an equal-power divider, as mentioned in [10]. When $J'_{12(1)}$ and $J'_{12(2)}$ are different, the divider becomes an unequal-power one. The ratio of $J'_{12(1)}$ and $J'_{12(2)}$ determines the power division of the two-way divider.

A circuit simulation of the networks in Fig.1 is carried out by AWR Microwave office in order to demonstrate the approach. The band-pass filter is designed at a center frequency of 3.5 GHz, with 0.3-dB ripple level, 2.5% fractional bandwidth and 50-Ω port impedance. The parameter values are obtained as follow [11]: $C_1 = C_2 = C_3 = 1$ pF, $L_1 = L_2 = L_3 = 2.067$ nH, $J_{01} = J_{34} = 2.8$ mS, $J_{12} = J_{23} = 0.4401$ mS, $J'_{12(1)} = J'_{12(2)} = J_{12}/\sqrt{2} = 0.3112$ mS (uniform power division), $J'_{12(1)} = 0.3651$ mS, $J'_{12(2)} = 0.2441$ mS (non-uniform power division). Here the admittance inverters J_{12}, $J'_{12(1)}$ and $J'_{12(2)}$ satisfy the relationship given in (3) and the ratio of $J'_{12(1)}$ and $J'_{12(2)}$ is 3/2. Fig. 2(a) demonstrates difference between the power divider and the third-order band-pass filter. From top to bottom the four simulated transmission losses at center frequency record, in order, 0 dB, -1.605 dB, -3.01 dB, -5.10 dB, which is just as expected. As seen, by setting the values of the admittance inverters as in equation (3), the appropriate power distribution can be obtained. Fig. 2(b) shows the phase responses of the two transmission paths of the non-uniform power divider. Obviously, the two transmission paths exhibit the same phase response. To summarize, as long as the admittance inverters are correctly designed, the two-way power divider can realize both the filtering and uniform/non-uniform power division function.

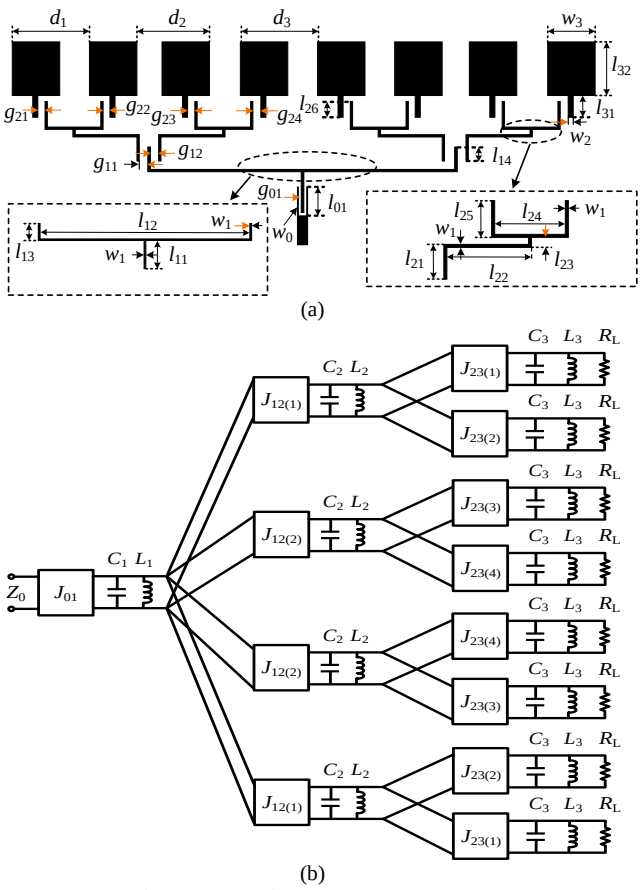

Fig. 3. Topology of the proposed filtering microstrip antenna array (a) and its equivalent circuit model (b).

Next, a new type of filtering antenna array with an eight-way power divider feeding network is proposed. The network is shown in Fig. 3(a). The whole geometry is bilaterally symmetrical and consists of three parts: (i) eight radiating patches, (ii) two different sizes of stub-loaded resonators (SLRs) [12], and (iii) one section of feeding microstrip line. Fig. 3(b) depicts the corresponding equivalent circuit. The two different sizes of SLRs and the radiating patches are modeled by parallel L_1C_1, L_2C_2, and $L_3C_3R_L$ resonators. The coupling gaps are modeled as the admittance inverters.

The values of lumped elements for the parallel L_1C_1, L_2C_2, and $L_3C_3R_L$ resonators are obtained by [10]

$$C_1 = C_2 = C_3 = \frac{g_3}{2\pi f_0 Z_0 \Delta} \tag{4}$$

$$L_1 = L_2 = L_3 = \frac{1}{4\pi^2 f_0^2 C_3} \tag{5}$$

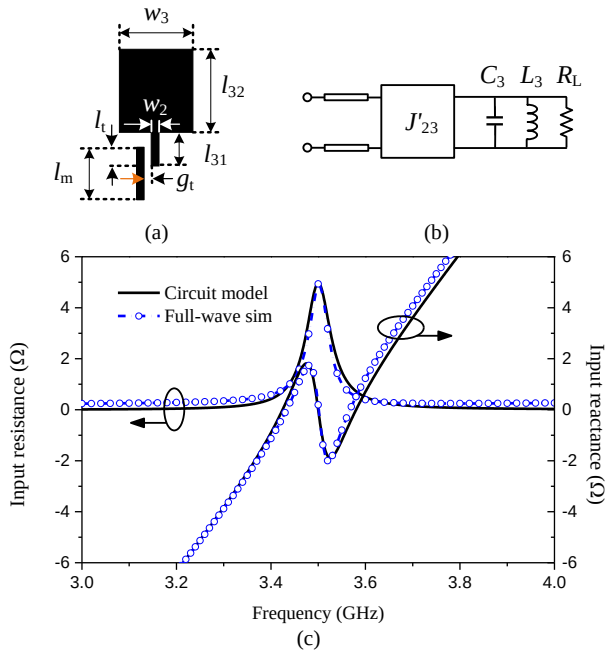

Fig. 4. Radiating patch extraction. (a) Test structure with l_m= 14.27, l_t = 6.3, g_t= 1, l_{31}= 9.45, l_{32}= 23.185, w_2= 2.2, w_3= 20.6, all in mm. (b) Equivalent lumped circuit with C_3 = 49.875 pF, L_3 = 41.46 pH, R_L = 50 Ω, J'_{23} = 6.3 mS. (c) Input impedances of the lumped circuit model and full-wave simulation.

where g_i is value of low-pass filter prototype element, Δ is the fractional bandwidth. According to the previous analysis and [11], the coupling parameters can be calculated utilizing the following equations

$$J_{01} = \sqrt{\frac{\Delta}{g_0 g_1}\frac{2\pi f_0 C_1}{Z_0}} \tag{6}$$

$$J_{12} = \sqrt{2J_{12(1)}^2 + 2J_{12(2)}^2} = 2\pi f_0 \Delta \sqrt{\frac{C_1 C_2}{g_1 g_2}} \tag{7}$$

$$J_{23} = \sqrt{J_{23(1)}^2 + J_{23(2)}^2} = \sqrt{J_{23(3)}^2 + J_{23(4)}^2} = 2\pi f_0 \Delta \sqrt{\frac{C_2 C_3}{g_2 g_3}} \tag{8}$$

The synthesis process requires the external quality factor (Q_{e1}) and coupling coefficients (M_{12} and M_{23}) [11]

$$Q_{e1} = \frac{1}{Z_0 J_{01}^2}\sqrt{\frac{C_1}{L_1}} = \frac{g_0 g_1}{\Delta} \tag{9}$$

$$M_{12} = \frac{J_{12}}{2\pi f_0 \sqrt{C_1 C_2}} = \frac{\Delta}{\sqrt{g_1 g_2}} \tag{10}$$

$$M_{23} = \frac{J_{23}}{2\pi f_0 \sqrt{C_2 C_3}} = \frac{\Delta}{\sqrt{g_2 g_3}} \tag{11}$$

The values of $J_{12(1)}$, $J_{12(2)}$ and $J_{23(1)}$ - $J_{23(4)}$ codetermine the final amplitude excitation of each radiating patch.

III. Design Procedure

The filtering antenna array in our work is chosen to be at a center frequency of 3.5 GHz, with third-order Chebyshev equal-ripple filter with 0.3-dB ripple level, 2.5% fractional bandwidth and 50-Ω port impedance. The design methodology

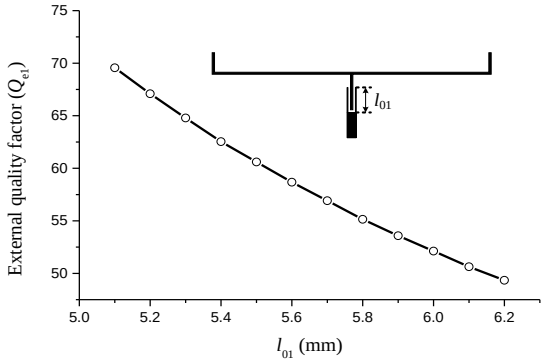

Fig. 5. Q_{e1} as the function of l_{01} and the test structure. l_{11} = 17.59, l_{12} = 118.2, l_{13} = 10.45, g_{01} = 0.2, w_0 = 0.4, w_1 = 1, all in mm.

described in this paper, although in principle narrow band, can be used to design wider-band components by using a substrate with lower dielectric constant and greater thickness [13]. The desired values can now be obtained according to (4)-(11): C_1 = C_2 = C_3 = 49.875 pF, L_1 = L_2 = L_3 = 41.46 pH, R_L = 50 Ω, J_{01} = 20 mS, J_{12} = J_{23} = 21.95 mS, Q_{e1} = 54.84, M_{12} = M_{23} = 0.02. Based on these parameters, the process microstrip resonator and patch design of the filtering microstrip antenna array will be discussed in detail next. The structure is printed on a substrate with dielectric constant ε_r=2.55, thickness h=0.8 mm, and loss tangent δ=0.0029. The full wave simulator Zeland IE3D has been used to carry out the EM simulation.

A. First- and Second-Stage Resonators Design

The first- and second-stage resonators can be viewed as stub-loaded resonators [12]. Since the open-circuited feeding stub is shunted at midpoint of the U-shaped microstrip line, the odd- and even-mode method [12] can be applied to analyze it. All the widths of the lines of the two resonators are selected the same. By properly choosing the lengths of the lines, the resonators can operate at any desired frequency.

B. Radiating Patch Design

The radiating patch is modeled by the shunt resonator with three parameters, R_L, L_3, and C_3 to be determined. The method of finding the circuit components is given in [10], which establishes a test structure to extract such equivalent circuit parameters by optimisation. Fig. 4(a) depicts the structure for extracting the equivalent circuit parameters of the radiating patch, and Fig. 4(b) show its equivalent circuit. The radiating patch is excited by one section of 50-Ω microstrip line with length l_m. The coupling between the microstrip line and the radiating patch is modeled by the admittance inverter J'_{23}.

Fig. 4(c) shows input impedances of both the full-wave and lumped-circuit model simulated result. The values of the lumped elements and the corresponding dimensions of the radiating patch are listed in the figure caption. Three parameters ($R_L L_3 C_3$) need to be determined. The patch width w_3 mainly affects the radiation resistance R_L. The stub length l_{31} and patch length l_{32} codetermine the resonant frequency (L_3 and C_3). As seen, the input impedances are well matched during the band of interest.

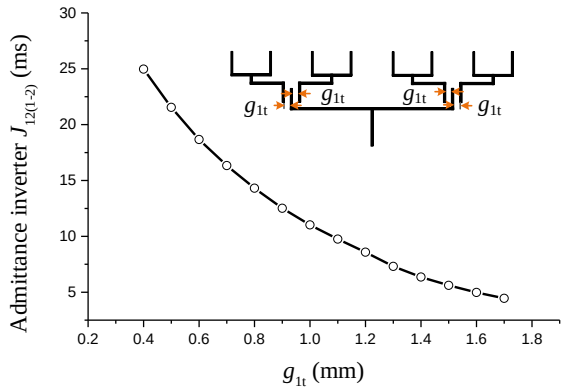

Fig. 6. $J_{12(1-2)}$ as the function of g_{1t} and the test structure. l_{14} = 7.3, l_{21} = 11.45, l_{22} = 27.8, l_{23} = 3.25, l_{24} = 23.2, l_{25} = 12.08, w_1 = 1, all in mm.

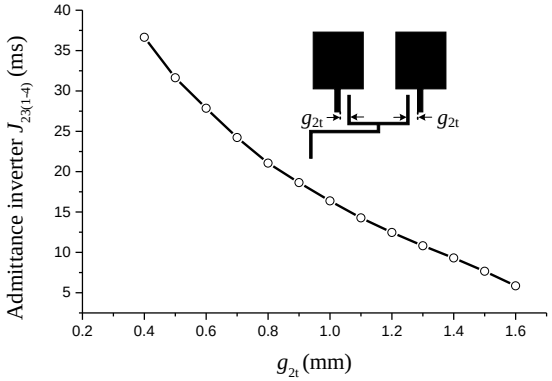

Fig. 7. $J_{23(1-4)}$ as the function of g_{2t} and the test structure. l_{26} = 7.6 mm.

C. External Quality Factor of the First-Stage Resonator

The first-stage resonator is fed by a 50-Ω microstrip line through the interdigital coupling. Fig. 5 depicts the test structure and the full-wave simulated Q_{e1} as a function of coupling length l_{01}.

D. Coupling Between the First Two-Stage Resonators

The structure for determining the coupling between the first and second stage resonators is presented in Fig. 6. The first-stage resonator is coupled with four second-stage resonators simultaneously. Our goal here is finding the curve of admittance inverter impedance versus different coupling gap. Therefore, during the extraction process, the coupling gaps are set as the same: $g_{11} = g_{12} = g_{1t}$. The relationship between $J_{12(1)}$ and $J_{12(2)}$ is thus defined as $J_{12(1)} = J_{12(2)} = J_{12(1-2)}$. Adjusting the gap size g_{1t}, the required M_{12} can be obtained. According to (7) and (10), $J_{12(1-2)}$ can be expressed in terms of M_{12}

$$J_{12(1-2)} = \pi f_0 \sqrt{C_1 C_2} M_{12} \tag{12}$$

Thus, the value of $J_{12(1-2)}$ versus different g_{1t} is obtained. Using Fig. 6, once we know the required values of $J_{12(1)}$ and $J_{12(2)}$, the corresponding coupling gap can be acquired.

E. Coupling between the Last Two-Stage Resonators

The extraction of coupling coefficient M_{23} is similar to that of M_{12}. Fig. 7 show the test structure and the extraction curve of the admittance inverter. Since the whole antenna structure is bilaterally symmetrical, only one group of the last two-stage resonators is needed to extract the M_{23}. Both the coupling gaps are set as g_{2t} and admittance inverters are set as $J_{23(1)} = J_{23(2)} = J_{23(1-4)}$. Appling (8) and (11), $J_{23(1-4)}$ could be expressed in terms of M_{23}

$$J_{23(1-4)} = \sqrt{2}\pi f_0 \sqrt{C_2 C_3} M_{23} \tag{13}$$

The value of $J_{23(1-4)}$ versus different g_{2t} is thus obtained. According to Fig. 7, once we get the values of $J_{23(1)}$-$J_{23(4)}$, the corresponding coupling gap could also be decided.

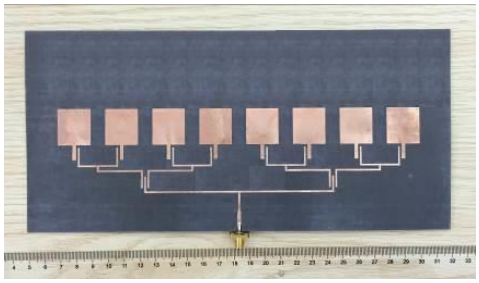

Fig. 8. Photograph of the fabricated filtering microstrip antenna array fed by a uniform power divider network.

Table I Some parameters of uniform filtering array (mm)

Parameter	l_{01}	g_{11}	g_{12}	g_{21}	g_{22}	g_{23}	g_{24}
Initiation	5.8	1	1	1.05	1.05	1.05	1.05
Optimization	5.7	1	1	1.15	1.15	1.15	1.15

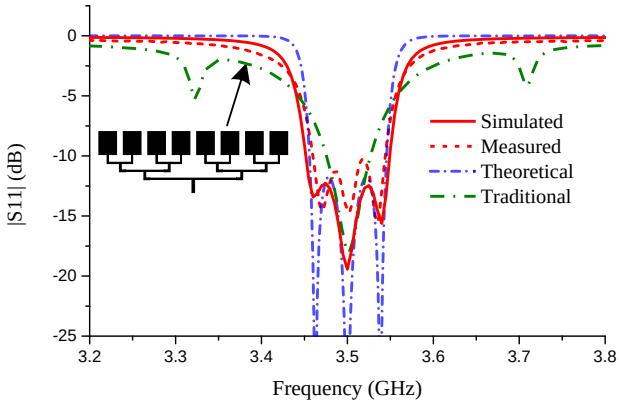

Fig. 9. |S11| comparison between the uniform filtering antenna array and the conventional patch antenna array.

IV. Example Filtering Antennas

In this section, two examples of third-order eight-element filtering antenna arrays with uniform and tapered power-distribution among the elements are designed, fabricated and measured.

A. Uniform Power Distribution

For the uniform power distribution, by applying (7) and (8), the admittance inverters are get as: $J_{12(1)} = J_{12(2)} = J_{12}/2$ = 10.98 mS, $J_{23(1)} = J_{23(2)} = J_{23(3)} = J_{23(4)} = J_{23}/\sqrt{2}$ = 15.52 mS. According to the Fig. 5, Fig. 6 and Fig. 7, the corresponding coupling length and gap can be obtained. A further full-wave optimization for fine tuning, focusing on the coupling strength, is carried out and the optimized parameters compared with the

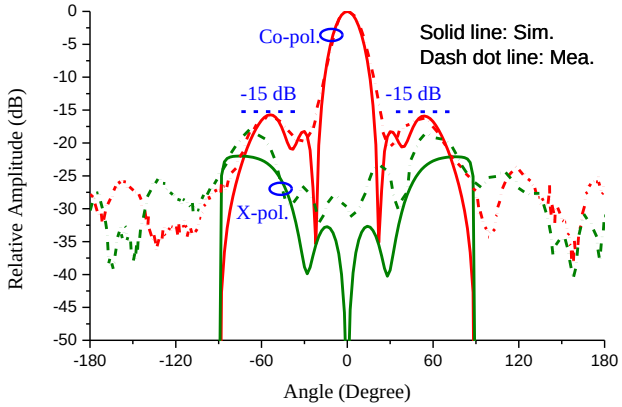

Fig. 10. Measured and simulated *H*-plane (yoz-plane) radiation patterns at 3.5 GHz.

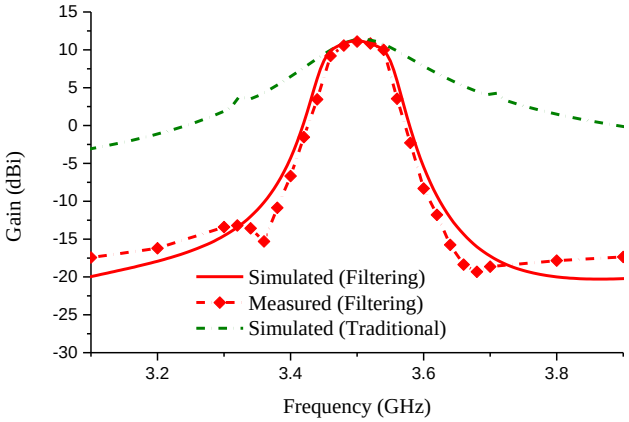

Fig. 11. Gain comparison between the filtering antenna array and the conventional patch antenna array.

initial ones are listed in Table I. The other dimension parameters of the filtering antenna array are listed as follows: l_{11} = 17.59, l_{12} = 118.2, l_{13} = 10.45, l_{14} = 7.3, l_{21} = 11.45, l_{22} = 27.8, l_{23} = 3.25, l_{24} = 23.2, l_{25} = 12.08, l_{26} = 7.6, l_{31} = 9.45, l_{32} = 23.105, w_0= 0.4, w_1= 1, w_2= 2.2, w_3= 20.6, g_{01} = 0.2, d_1 = 29.7, d_2 = 29.9, d_3 = 29.9 (all values in mm). Minor difference between the initial and optimized antenna performances is found in our design.

Fig. 8 shows the photograph of the filtering antenna array fed by the uniform resonator based power divider network. The theoretical, simulated and measured |S11| of the filtering antenna array in comparison with a traditional patch array (with no filtering) is depicted in Fig. 9. As lossless lumped-element equivalent circuit (*LC* resonator) is used to acquire theoretical results, slight difference between theory and simulation (lossy microstrip circuit) can be observed. The traditional patch array is printed on the same substrate, dielectric constant of 2.55 and thickness of 0.8 mm. The patches of the traditional patch array are fed by a non-filtering uniform power divider and the other parameters of the two patch arrays are identical. As seen, three reflection zeros are clearly visible for the integrated antenna array demonstrating the expected third-order filtering response. For the traditional patch array, only one resonant mode can be observed within passband. The measured -10 dB reflection bandwidth of the filtering antenna array is much wider than its traditional simulated counterpart. Minor discrepancy between

Table II Some parameters of non-uniform filtering array (mm)

Parameter	l_{01}	g_{11}	g_{12}	g_{21}	g_{22}	g_{23}	g_{24}
Initiation	5.8	1.2	0.85	1.1	1	1.1	1
Optimization	5.7	1.4	0.8	1.25	1	1.2	1.1

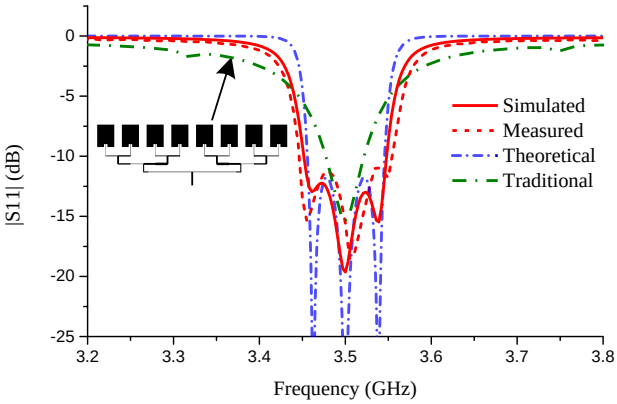

Fig. 12. |S11| comparison between the non-uniform filtering antenna array and the conventional patch antenna array.

the measured and simulated results can be attributed to the fabrication error. Although a filter can be placed at the input to the traditional array to achieve a similar selectivity, this increases the size of the structure and also maybe degrades the in-band performance as mentioned in introduction.

Fig. 10 shows the normalized simulated and measured radiation patterns of the filtering antenna array. The patterns of *E*-plane are similar to those of the traditional patch antenna, thus only the patterns of *H*-plane are presented. Besides, due to the infinite ground setup in IE3D, only the ±90º regions of the simulated radiation patterns are plotted. The patterns exhibit expected radiation performance with maximum antenna gain in the broadside. The measured sidelobe level achieves -15.6 dB at the design frequency. The relatively large cross-polarized radiation in the large-angle region is induced by the strong horizontal currents of the resonators under the resonant state.

Fig. 11 shows the measured and simulated realized antenna gains of the proposed filtering antenna array. The simulated gain of the traditional antenna array is also included for comparison. The maximum gain at the center frequency is measured as 11.1 dBi. For the proposed filtering antenna array, the gain drops sharply outside the band of the included filter. The suppression level outside the passband of the filtering antenna array is recorded over 15 dB higher than that of the traditional antenna array. Thus, without using cascaded band-pass filter, the integrated design improves the suppression level outside the passband significantly.

B. Tapered Power Distribution

For the tapered power distribution, a 20-dB 8-element Dolph-Tschebyscheff synthesis [13] is adopted for the tapering of the the power amplitude values. Different coupling gaps are used to obtain the required power-split. The required amplitude weight vector is [1, 1.1386, 1.5091, 1.7244]. The ratio of $J_{23(1)}$ squared and $J_{23(2)}$ squared as well as the ratio of $J_{23(3)}$ squared and $J_{23(4)}$ squared are: $J^2_{23(1)}$ / $J^2_{23(2)}$ =1/1.1386^2, $J^2_{23(3)}$ / $J^2_{23(4)}$

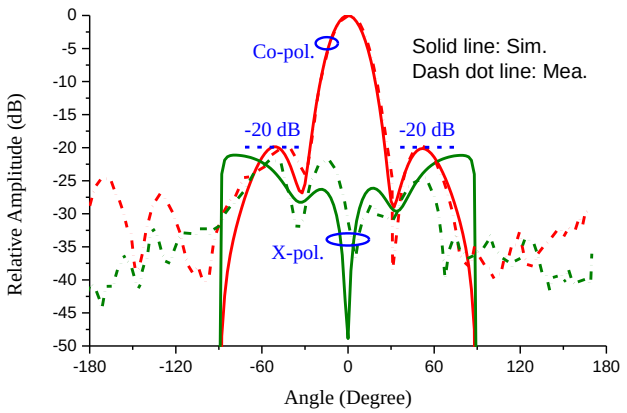

Fig. 13. Measured and simulated *H*-plane (yoz-plane) radiation patterns at 3.5 GHz.

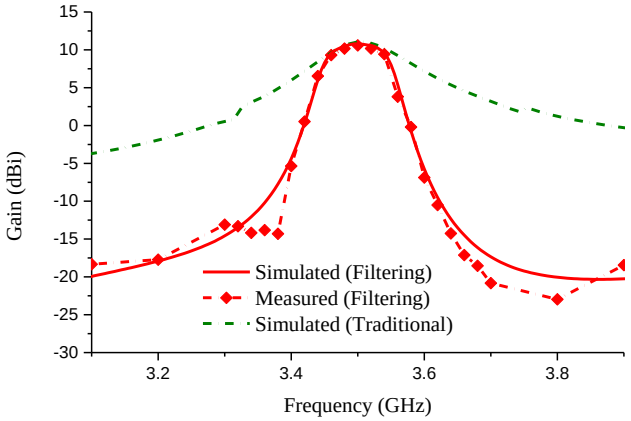

Fig. 14. Gain comparison between the proposed filtering antenna array and the conventional patch antenna array.

$=1.5091^2/1.7244^2$. The ratio of $J_{12(1)}$ squared and $J_{12(2)}$ squared is: $J^2_{12(1)}$ / $J^2_{12(2)}$ $=(1+1.1386^2)/(1.5091^2+1.7244^2)$. Appling (7) and (8), the admittance inverters can be calculated as: $J_{12(1)}$ = 8.56 mS, $J_{12(2)}$ = 12.95 mS, $J_{23(1)}$ = 14.49 mS, $J_{23(2)}$ = 16.49 mS, $J_{23(3)}$ = 14.46 mS, $J_{23(4)}$ = 16.52 mS. According to Fig. 6 and Fig. 7, the initial corresponding coupling gap can be obtained. The optimized parameters compared with the initial ones are listed in Table II. The other dimension parameters of the filtering antenna array are as follows: d_1 = 29.65, d_2 = 30.2, d_3 = 30.4 (all values in mm). The parameters not mentioned are the same with those in the above antenna array fed by a uniform power divider network.

The fabricated prototype of non-uniform filtering array is almost the same with the uniform one except the coupling section. The comparison between the filtering antenna array and a conventional patch antenna array with taper-amplitude excitation is presented. As seen from Fig. 12, the measured -10 dB impedance bandwidth of 2.86% from 3.45 GHz to 3.55 GHz is achieved, still much wider than its traditional simulated counterpart.

As seen fom the Fig. 13, the sidelobe level in the measured H-plane achieves -19.7 dB, 4.1 dB lower than that of the antenna array with uniform-amplitude excitation. In the case of non-uniform feeding, symmetries are introduced and the radiation due to the horizontal currents in the feeding network can't well cancel out, which leads to larger cross-polarization level than that in the case of uniform feeding. The gain response is shown in Fig. 14. The maximum gain at the center frequency is measured as 10.6 dBi, slightly lower than the uniform array as expected. The simulated antenna efficiency of the non-uniform filtering antenna array at center frequency is 55%, which can be improved by using a substrate with smaller δ, lower ε_r, and greater h [13]. If the proposed antenna is developed on a substrate with ε_r=2.55, h=0.8 mm, and δ=0.0004, the simulated efficiency is 74%, close to that in [10] (72.2%). The antenna array fed by an amplitude-tapering network shows not only the good filtering response but also the low sidelobe level.

V. Conclusion

This paper introduces a design of filtering microstrip antenna array with reduced sidelobe level. Two filtering microstrip antenna arrays fed by a uniform/non-uniform power divider network have been designed, fabricated and measured. Both the antenna arrays achieve good impedance matching characteristic as well as filtering response showing a flat gain frequency response, sharp band-edge characteristic, and high stop-band suppression. The filtering antenna array fed by a non-uniform power divider presents low sidelobe performance. The proposed approach and idea would be useful to design of larger scale of filtering and low sidelobe antenna arrays.

References

[1] W.-J. Wu, Y.-Z. Yin, S.-L. Zuo, Z.-Y. Zhang, and J.-J. Xie, "A new compact filter-antenna for modern wireless communication systems," *IEEE Antennas Wireless Propag. Lett.*, vol. 10, pp. 1131-1134, 2011.

[2] C.-T. Chuang and S.-J. Chung, "Synthesis and design of a new printed filtering antenna," *IEEE Trans. Antennas Propag.*, vol. 59, no. 3, pp. 1036–1042, Mar. 2011.

[3] T. L. Nadan, J. P. Coupez, S. Toutain, and C. Person, "Optimization and miniaturization of a filter/antenna multi-function module using a composite ceramic-foam substrate," in *IEEE MTT-S Int. Microw. Symp. Dig.*, Jun. 1999, pp. 219–222.

[4] C.-K. Lin and S.-J. Chung, "A compact filtering microstrip antenna with quasi-elliptic broadside antenna gain response," *IEEE Antennas Wireless Propag. Lett.*, vol. 10, pp. 381-384, 2011.

[5] X. W. Chen, F. X. Zhao, L. Y. Yan, and W. M. Zhang, "A compact filtering antenna with flat gain response within the passband," *IEEE Antennas Wireless Propag. Lett.*, vol. 12, pp. 857-860, 2013.

[6] Y. Yusuf and X. Gong, "Compact low-loss integration of high-Q 3-D filters with highly efficient antennas," *IEEE Trans. Microw. Theory Tech.*, vol. 59, no. 4, pp. 857–865, Apr. 2011.

[7] C.-Y. Hsieh, C.-H. Wu, and T.-G. Ma, "A compact dual-band filtering patch antenna using step impedance resonators," *IEEE Antennas Wireless Propag. Lett.*, vol. 14, pp. 1056-1059, 2015.

[8] X. Y. Zhang, W. Duan, and Y. M. Pan, "High-gain filtering patch antenna without extra circuit," *IEEE Trans. Antennas Propag.*, vol. 63, no. 12, pp. 5883–5888, Dec. 2015.

[9] C.-X. Mao, S. Gao, Y. Wang, F. Qin, and Q.-X. Chu, "Multimode resonator-fed dual-polarized antenna array with enhanced bandwidth and selectivity," *IEEE Trans. Antennas Propag.*, vol. 63, no. 12, pp. 5492–5499, Dec. 2015.

[10] C.-K. Lin and S.-J. Chung, "A filtering microstrip antenna array," *IEEE Trans. Microw. Theory Tech.*, vol. 59, no. 11, pp. 2856–2863, Nov. 2011.

[11] J. S. Hong and M. J. Lancaster, *Microstrip Filters for RF/Microwave Applications*. New York: Wiley, 2001.

[12] X. Y. Zhang, J.-X. Chen, Q. Xue, and S.-M. Li, "Dual-band bandpass filters using stub-loaded resonators," *IEEE Microw. Wireless Compon. Lett.*, vol. 17, no. 8, pp. 583–585, Aug. 2007.

[13] C. A. Balanis, *Antenna Theory*, 2nd ed. New York: Wiley, 1997.